# Mobile Battery Storage Modeling and Normal-Emergency Operation in Coupled Distribution-Transportation Networks

Hedayat Saboori, Hasan Mehrjerdi , Senior Member, IEEE, and Shahram Jadid

 $\zeta_{(i,t)}$   $E_{Tot}^{Shed}$ 

 $P_{(b,i,t)}^{Ch}, P_{(b,i,t)}^{Di}$ 

 $\begin{array}{l} P^F_{(i,j,t)}, Q^F_{(i,j,t)} \\ Q^{Ca}_{(b,i,t)}, Q^{In}_{(b,i,t)} \end{array}$ 

 $X_{(b,i,t)}^{PC}, X_{(b,i,t)}^{PD}$ 

 $Y_{(b,i,t)}^{QI}, Y_{(b,i,t)}^{QC}$ 

 $J_{(b,t)}^{MB} \\ V_{(\underline{i},t)}$ 

 $P_{(i,t)}^R, Q_{(i,t)}^R$ 

Abstract—Previous research has proved that Mobile Battery Energy Storage (MBES) can play a pivotal role in achieving resiliency goals in distribution networks besides sustainability purposes. The missing links in the practical deployment of this new flexibility resource are the discontinuity between normal and emergency operating states in addition to the high computational burden. Accordingly, a new rolling-horizon operation model for a fleet of truck-mounted mobile batteries (TMMBs) employed in a joint transportation-distribution network is proposed. The model can effectively handle and switch between normal and emergency states by integrating a new schedule memory concept into the upcoming horizons. The spatial and temporal dynamics of the TMMBs, along with the transportation time and cost constraints, are modeled by a novel linear and computationally affordable formulation. The model runtime is further targeted by proposing a two-stage optimization model to detach transportation network calculations from the distribution grid. Additionally, a lexicographic multi-objective paradigm is used to ensure a maximum resiliency plan at the minimum expenses during emergencies. The model considers outage and congestion change of the road traffic beyond the forecasted values besides network uncertainties. Implementing the model on a test case proves its functionality in dealing with diverse network situations.

Index Terms—Distribution network, multi-stage lexicographic programming, mobile battery, resiliency, rolling horizon.

Sets	Nomenclature
$A_B$	Mobile batteries.
$A_I$	Network buses.
$A_M$	Flow linearization segments.
$A_T$	Time periods.
Parameters	
$TTT_{(i,j)}$	Total transportation time.

Manuscript received 23 January 2022; revised 8 May 2022; accepted 7 June 2022. Date of publication 11 July 2022; date of current version 20 September 2022. This work was supported by the National Priorities Research Program through the Qatar National Research Fund under Grant 11S-1125-170027. Paper no. TSTE-00074-2022. (Corresponding author: Hasan Mehrjerdi.)

Hedayat Saboori is with the Electrical Engineering Department, Kermanshah University of Technology, Kermanshah 83GW+3H3, Iran (e-mail: hedayat. saboori@qu.edu.qa).

Hasan Mehrjerdi is with the Electrical Engineering Department, Qatar University, Doha 9FGR+WF7, Qatar (e-mail: hasan.mehrjerdi@qu.edu.qa).

Shahram Jadid is with the Electrical Engineering Department, Iran University of Science and Technology, Tehran 16844, Iran (e-mail: jadid@iust.ac.ir).

Color versions of one or more figures in this article are available at https://doi.org/10.1109/TSTE.2022.3189838.

Digital Object Identifier 10.1109/TSTE.2022.3189838

$\rho$	Transportation cost per nour
$\psi_{(t)}$	Operation status indicator.
$\psi_{(t)} \\ \lambda_{(n)}^S, \ \gamma_{(n)}^R$	Substation and renewable cost coeffi-
	cient.
$P_{(i,t)}^{D}, Q_{(i,t)}^{D} $ $\eta_{(b)}^{Ch}, \eta_{(b)}^{Di}$	Active and reactive bus demand.
$\eta^{Ch}_{(b)},\eta^{Di}_{(b)}$	Charging and discharging efficiency of battery.
aMP -Min -Man	
$S_{(b)}^{MB}, E_{(b)}^{Min}, E_{(b)}^{Max}$	Power and energy limitations of battery.
$R_{(i,j)}^F X_{(i,j)}^F S_{(i,j)}^F$	Resistance, reactance, and rating of the
( 12 / ( 12 / ( 12 /	line.
$V_{Min}^{Bus}, V_{Max}^{Bus}$	Upper and lower limit of voltage mag-
	nitude.
$P_{R(i,t)}^{Max}, PF_{(i)}^{R}$	Generation limit and power factor of
	renewables.
Variables	
$\Omega_{(b,i,t)}^{MB}$	Binary status variable of the batteries.
. – a	

Transportation cost per hour

Binary status variable of the batteries. Substation generated power block. Bus load shedding binary indicator. Total recoverable load during emergen-

Charging and discharging active power of battery.

Active and reactive flow of the line.

Capacitive and inductive reactive power of battery.

Active and reactive power generation of renewables.

Binary charging and discharging active indicators.

Binary capacitive and inductive reactive indicators.

Stored energy in the battery.

Bus voltage magnitude. Curtailed power of the renewable re-

source.

## I. Introduction

R ECENT trends of sector coupling and electrification exacerbate our dependency on continuity of electricity supply causing the spread of outages impacts [1]. Concurrently, promoting customer participation via demand response programs in the context of smart grid initiatives has increased the

1949-3029 © 2022 IEEE. Personal use is permitted, but republication/redistribution requires IEEE permission. See https://www.ieee.org/publications/rights/index.html for more information.

penetration of monitoring and control technologies. The reliance of these technologies on advanced communication networks and information systems has made the energy infrastructure further susceptible to cybersecurity threats and attacks [2]. At the same time, the climate change consequences intensify the probability of major disruptive events [3]. The superposition of these factors is becoming a driving force to augment the resilience of the energy infrastructure, especially distribution networks. Energy storage systems are widely recognized for their capability to enhance energy resilience [4]. Specifically, battery energy storage systems (BESS) increase resilience by providing local electric service through an outage and enabling renewable generators to produce power through outages [5]. Most BESS solutions are currently stationary, interconnected with permanent infrastructure, and designed to serve localized loads [6]. On the contrary, the ability of the Mobile Battery Energy Storage (MBES) to relocate in the grid provides enhanced advantages over the stationary counterpart. This flexibility, the principal advantage of MBES, provides connection changeability as conditions on the grid change over time in both normal and emergency situations [7]. This feature is specifically an advantage during outage conditions [8]. The nature of many outages is that they cannot be completely anticipated. In this case, the operator can benefit from the MBES by the exact location of the emergency power requirement. Furthermore, mobile storage can retrieve excess renewable energy exposed to curtail due to the various technical and economic limitations. This is especially the case for the curtailments resulting from the spatiotemporal constraints [9], [10].

Accordingly, the modeling and operational planning of the MBES for normal and emergency states have been the focus of research in the past decade. In [11], a model is proposed for the optimized investment of MBES in the distribution networks considering normal and emergency operation. The proposed two-stage model defines the optimal capacity of the mobile batteries in the first stage and then reschedules the installed assets optimally in the second stage. The computational burden of the model is high, and as a result, the authors have applied the progressive hedging algorithm to solve the problem. The authors in [12] have coordinated the repair crew with the MBES to cope with distribution network disasters. The model is convexified and then linearized to be solvable with off-the-shelf packages. In a similar work in [13], the repair crew is coordinated with the mobile generators and batteries for optimal service restoration in reconfigurable distribution networks. The authors have used the traditional time-space network model to handle the spatiotemporal nature of mobile resources. Since the high computational burden, the Floyd-algorithm-based time-space simplification method is utilized to solve the problem. In [14], a rolling horizon operation model for optimal distribution network restoration employing MBES fleet and resource dispatch in microgrids is proposed. The proposed model considers damage to both the transportation network and distribution grid while uncertainties in load demand and availability of branches are considered using Monte Carlo simulation. The authors in [15] have proposed a two-stage operation model wherein the mobile resources are prepositioned before the disaster. The mobile resources are

dynamically scheduled in the second stage to achieve an optimal restoration plan. In [16], both stationary and mobile storage has been used in a three-layer multi-agent model comprising cyber, physical, and transportation layer. In [17], a coordinated post-disaster restoration procedure employing mobile batteries in distribution networks integrating multi-microgrids is proposed. The total system cost is minimized, including unmet load, generation cost, and mobile battery operation costs. The authors in [18] have benefited from the spatial flexibility of mobile batteries for agile restoration of distribution grid to cope with consequences of high-impact low probability (HILP) incidents. Accordingly, a stochastic, non-linear, and non-convex model with joint probabilistic constraints (JPCs) is developed and then reformulated to a tractable mixed-integer linear programming (MILP). Finally, the flexibility of power transactions and the multi-microgrids and MBES is coordinated in [19], wherein the expected-power-not-served and expected-power-curtailment are derived as the risk measures.

Most of the previous research investigating MBES has utilized a spatiotemporal operation model involving different variables for each connection and transportation state. Based on this differentiation, many constraints have been used to model the MBES behavior. These features and the inherent high-dimensionality resulting from spatiotemporal nature have made the developed models computationally intensive and thus time-consuming. This issue will be particularly problematic in emergencies with severe runtime constraints. Besides, most of the previous studies on MBES are based on a coupled model for transportation and distribution networks. In other words, the minimum travel distance between possible bus candidates has to be calculated at any model run. This issue increases solution runtime in the cases without changes in the transportation network routes, connections, or congestion. The increased runtime resulting from the current MBES literature practice is significantly exacerbated in the context of uncertainty management reformulations. Last but not least, much of the MBES research has focused on developing a model for one of the operations states, i.e., normal or emergency. Neglecting state changeability limits the functionality of the developed models to hypothetical single-state situations rather than real-life conditions with a high likelihood of unanticipated state switching.

Accordingly, a scheduling model is proposed in this paper for optimal MBES operation in distribution networks. The proposed model splits the transportation network from the core MBES scheduling by employing a two-stage model. Then, based on the network situation, the model will handle and switch between normal and emergency conditions. Achieving the maximum network resiliency at a minimum operational expense is then guaranteed through a lexicographic procedure during emergencies. The proposed scheduling paradigm benefits from a novel MBES spatiotemporal model involving transportation time and cost constraints with a linear and low computational burden formulation. The inherent parameter uncertainties and unforeseen events are also addressed using a new schedule memory concept-based rolling horizon procedure. Having this feature, the model can consider transportation network outages and congestion changes beyond the forecasted values besides

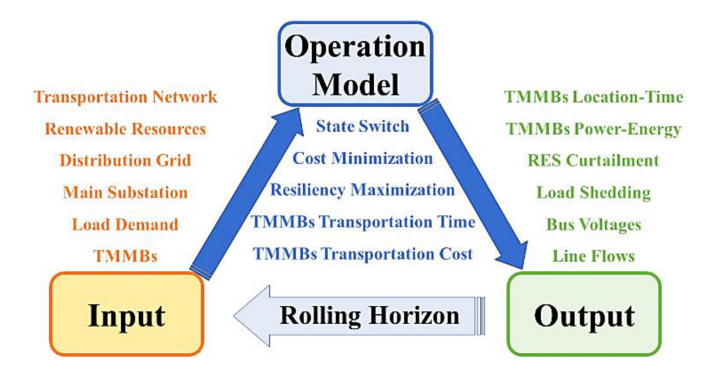


Fig. 1. General concept of the TMMBs operation is coupled distribution-transportation network.

distribution grid uncertainties and outages. In summary, the paper contributions are as follows:

- Proposing a hybrid and switchable normal-emergency operation paradigm based on a two-stage and lexicographic procedure ensuring maximum resiliency at minimum operating expenses during disasters.
- 2) Developing an efficient and low computational burden linear spatiotemporal model for mobile batteries taking transportation time and cost into account
- Integrating the impact of the transportation network and distribution grid outages and forecast errors via a new rolling horizon model deploying a novel schedule memory concept.

The remaining parts of the paper are organized as follows: Section II introduces the conceptual and mathematical model of the proposed model. Section III presents the results of implementing the model on a test case. Lastly, Section IV draws the concluding remarks and drives trends for future works.

#### II. PROPOSED MODEL

The mobile energy storage systems are mobilized grid-scale battery systems employed in transmission or distribution networks [20]. The whole battery system comprising storage cells, power converter, and transformer (high voltage connection) is compacted and containerized, suitable for truck or train transportation [21]. Although a fleet of truck-mounted mobile battery (TMMB) systems is considered here, the proposed model is general enough to be used in any other cases [22]. At specific points where the transportation network coincides with the distribution grid and sufficient space for parking is available, the TMMB can connect to a network bus. The dynamic bus location of the TMMBs offers unprecedented flexibility to the network operator, especially in distribution networks. Exploring this potential is targeted in the following by modeling the TMMBs' spatiotemporal dynamics besides technical constraints.

Fig. 1 demonstrates the general concept and integral parts of the targeted problem. As in the figure, there is an electrical power distribution network coupled with a road transportation network. The distribution network is supplied from a main upstream sub-transmission substation. Besides, some renewable and distributed generation resources are connected to network

buses. This renewable-integrated and coupled distributiontransportation network aims at supplying load demand. The above-described network benefits from a fleet of TMMBs capable of moving between network buses and changing connection locations. Parameters and assumptions related to the distribution grid, transportation network, renewable resources, main substation, load demand, and TMMBs constitute inputs of the problem, namely optimal network operation. These values are entered into an optimization problem to achieve defined operation objectives while observing various constraints. One of the main features of the proposed model is the ability to switch instantly between various operation states of the distribution network, i.e., normal and emergency. Central to these operation states, minimizing the total operation cost and maximizing the network resiliency are addressed. To this end, a new efficient and linear mathematical model is proposed to consider real-life constraints related to the TMMBs' transportation time and cost. Once the problem is solved, network variables will be defined. The main variables of the problem are the spatial-temporal and power-energy status of the TMMBs.

Accordingly, curtailed renewable energy at both normal and emergency operation state and unmet load at the emergency state will be defined. Finally, the value of the bus voltages and line flows are known. If the network state changes due to a natural disaster or a fault situation, some of these outputs will be fed back to the problem as input parameters, described in the following. This rolling horizon paradigm helps to switch instantly between two operation states when needed.

The general logic of the proposed scheduling method for both normal and emergency operation states is depicted in Fig. 2. As in the figure, the proposed operation paradigm comprises three parts, First Stage, Second Stage, and Schedule Memory. In the first stage, an initial preprocessing has to be performed. This stage excludes transportation network calculations from the central TMMBs scheduling. As in the figure, this stage will be repeated if there are changes in the transportation network connections or congestion. This feature means that the related calculations are not necessarily involved in every model run resulting in a lower computational burden. Then, the TMMBs will be scheduled based on the network situation in the second stage, namely normal or emergency operation state. The results of the last model run are then practically implemented at the current time period after defining and saving the schedule memory. The operation schedule for the forthcoming period will be decided according to the new information received during the same period. For this purpose, three investigations will be made based on the new information received. The first investigation compares the status of the transportation network in the upcoming period with the previous one. If there are changes in the form of road disconnection or congestion changes, the First Stage has to be simulated. Then, the network operation state will be decided at the Second Stage based on the second and third investigations. The second investigation denotes checking outage of the distribution lines or power sources, including distributed generators and/or main substation. This situation indicates probable load shedding because of generation inadequacy or island formation. If the above situation is the case, the model is directed

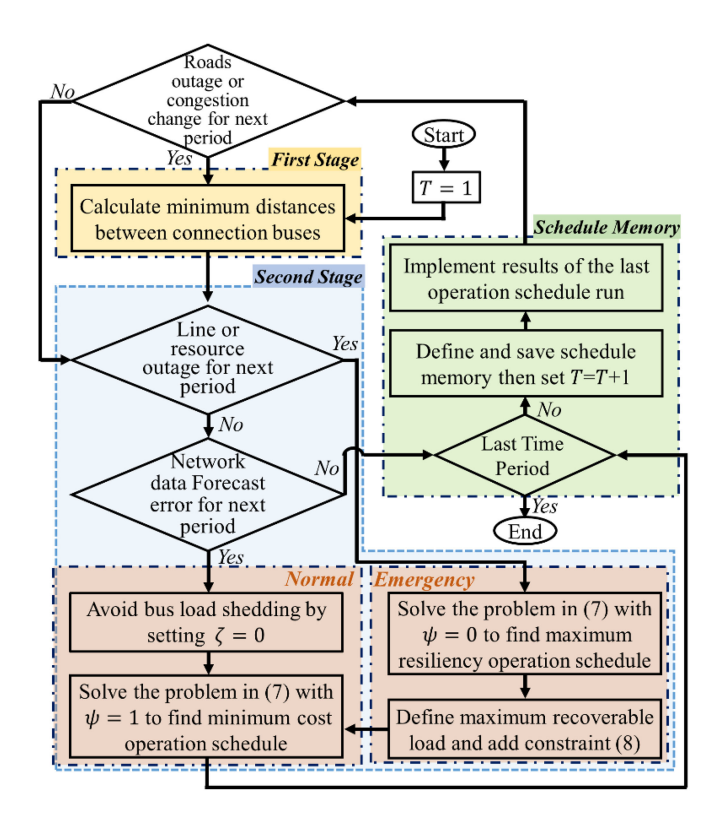


Fig. 2. Flowchart of the proposed method for TMMBs operation.

to the *Emergency* operation schedule. Otherwise, the *Normal* operation schedule is selected due to observing errors in the forecasted network data, for instance, load demand or renewable generation. Irrespective of the network operation state, this cyclic operation paradigm will be counted and continued until the last time. The process is terminated by reaching the last defined time period, as seen in Fig. 2.

Before approaching the following time period, the schedule memory has to be first saved, and then in case of receiving new information or network changes, the program will be rerun for the next time period. Otherwise, the last obtained results will implement until new information is received. Details of each operation stage, in addition to the TMMBs spatiotemporal model and operation schedule, are provided in the following.

#### A. First Stage: Minimum Distance Calculation

Fig. 3 depicts a generic coupled distribution-transportation network with TMMBs. As in the figure, there are some road parking points and some connection points. As declared before, the connection points denote the coincidence location of both networks possessing the required parking location for the TMMB truck. These points are the only locations where the truck can park to connect the battery to one of the network buses. The time required to change the connection of the TMMBs between network buses depends on three factors, the time required to disconnect the existing connection (TD), move between network buses (TM), and reconnect to the new bus (TC). Therefore, the required time for each possible transportation can be calculated by minimizing the sum of the abovementioned three times to

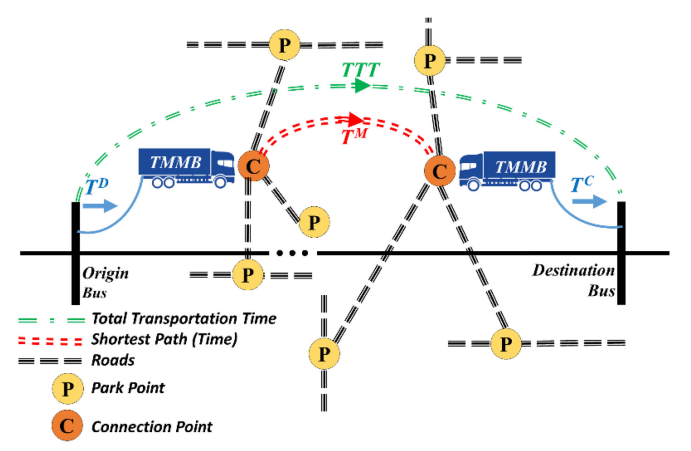


Fig. 3. A generic coupled distribution-transportation network with TMMBs.

achieve the Total Transportation Time (TTT), as in (1).

$$TTT_{(i,j)} = \min \ \left( T_{(i)}^D + T_{(i,j)}^M + T_{(j)}^C \right) \ \forall \ \{i,j\} \in A_I \quad (1)$$

The time of disconnection and reconnection are predefined and constant values for all possible transportations. However, the movement time of the TMMBs is a function of the transportation network configuration and its congestion and varies from case to case. As a result, the TTT in (6) can be rewritten as:

$$TTT_{(i,j)} = \left(T_{(i)}^D + T_{(j)}^C\right) + \min T_{(i,j)}^M \ \, \forall \ \, \{i,j\} \in A_I \ \, (2)$$

Typically, there are several paths for moving between two buses. However, the shortest route for each possible movement can be obtained from the currently developed algorithms, for example, the shortest path algorithm. The minimum transportation time between connection buses can be calculated utilizing this method at the beginning of the daily operation schedule. The result then has to be added to the detachment and attachment time of the TMMBs to calculate the TTT, as shown in (2). The results for all transportations between network buses with a connection point can be simply represented by the Total Transportation Time Matrix (TTTM). Each row and column in the constructed TTTM denote each connection point's distances to other connection points.

This matrix can be simply calculated ahead of the main scheduling module. Excluding the required calculation time of the TTTM from the scheduling will help reduce the execution time in the receding horizons, especially those without transportation network changes or damages. In other words, the TTTM will only be recalculated when the road lines are damaged or their traffic does not meet the predicted patterns. The TTTM calculated in this step will then be used for optimal scheduling of the TMMBs.

## B. Spatial and Temporal Dynamics of the TMMBs

Each TMMB can change its bus connection if and even if the TTT between origin and destination buses is expired at future consecutive time periods. To model this situation, it is considered that each TMMB will adopt one of the connection or transportation modes. The connection mode is shown with a three-dimensional binary variable as follows.

$$\Omega_{(b,i,t)}^{MB} \in \{0,1\} \ \forall \ b \in A_B, \ i \in A_I, \ t \in A_T$$
 (3)

If mobile battery b is connected to bus i at time period t, then the corresponding status binary value is equal to one; otherwise, it is zero. It should be noted that the mobile battery can only connect to one of the network buses at any given time, which is modeled by (4).

$$\sum_{i} \Omega_{(b,i,t)}^{MB} \le 1 \quad \forall \ b \in A_B, \ t \in A_T \tag{4}$$

Unlike the previously proposed models, battery transportation mode is also defined based on the binary status variable to avoid increasing the number of decision variables. Accordingly, when the value of this variable is zero for all network buses for a specific time period, it is considered that the battery is moving. This rule is used to formulate the transportation time limit. In other words, if a TMMB is currently connected to a bus, it can only change its connection at future time intervals if the transportation time required to move is elapsed. This situation means that the transportation status of the battery can be modeled by its not-connection status. This limitation is modeled by only one inequality as follows.

$$\Omega_{(b,i,t)}^{MB} + \Omega_{(b,j,u)}^{MB} \le 1$$

$$\forall b \in A_B, t \in A_T, \{i,j\} \in A_I, i \neq j,$$

$$u = \left\{t + 1, \dots, t + TTT_{(i,j)}\right\}$$
(5)

Based on this inequality, the battery can only change its bus connection location if it will not be connected to any network buses at future intervals, at least to the extent of the total transportation time between origin and destination buses. The problem with this inequality is that the battery may not necessarily connect to the destination bus after passing the required, leaving it in neither connection nor transportation mode. This problem is handled in the following by linking the transportation cost to the non-connection times of the battery. The transportation cost of the TMMB is related to the truck's fuel consumption, which is, in turn, a function of the transportation time. Accordingly, the transportation hours of the TMMB can convert into its transportation cost by multiplying the fuel cost of each driving hour, as follows.

$$TC_{(b,t)}^{MB} = \beta \left( 1 - \sum_{i} \Omega_{(b,i,t)}^{MB} \right) \quad \forall \ b \in A_B, \ t \in A_T \quad (6)$$

The above equation denotes that there will be a transportation charge for each hour that the battery is not connected to any of the network buses, meaning its transportation. Since this cost term will be included in the objective function, the solving procedure will minimize its value by removing unnecessary non-connection periods. This, in turn, means that the battery will connect to one of the network buses immediately after elapsing the required transportation time when changing the connection location.

#### C. Second Stage: Normal Operation

As in Fig. 1, after calculating the TTTM in the case of changes in the transportation network, the new information received is evaluated to decide the network operation status. If the network conditions change, the model will be resolved again. The network changes may be in the form of forecasting errors or equipment outages. In this case, the model is resolved considering new data for the upcoming time period. Based on the level of the changes, the network operation state will fall into normal or emergency. The normal operation state denotes encountering errors in the forecasted values comprising network data without power generation or load supply deficiency. For the *Normal* operation state, the course of the commands is based on the following objective function.

$$\min \begin{bmatrix} \psi_{(t)} \left( \sum_{t} \sum_{n} \lambda_{(n)}^{S} \Delta P_{(n,t)}^{S} + \sum_{i} \sum_{t} \gamma_{(n)}^{R} P_{(i,t)}^{R} \right) \\ + \beta \sum_{b} \sum_{t} \left[ 1 - \sum_{i} \Omega_{(b,i,t)}^{B} \right] \\ - \left( 1 - \psi_{(t)} \right) \sum_{i} \sum_{t} \left( 1 - \zeta_{(i,t)} \right) P_{(i,t)}^{D} \end{bmatrix}$$
(7)

Based on the above objective function, switching the value of  $\psi$  to one, in the normal operation state, will return a cost-only objective function equal to the first term of (7). The important note to be declared here is that the load shedding is not allowed in this operation state by turning the value of  $\zeta$  for all network buses and time periods to zero, discussed further in the following. The first term of (7), activating for the normal operation state, accounts for the total operation cost comprising substation and renewable resources energy cost in addition to the transportation cost of the TMMBs. A stair-wise cost function is used to model substation energy cost. Additionally, renewable resources offer their power based on a linear cost function. The transportation cost of the whole TMMBs fleet is also calculated by elaborating (6) over whole time periods and mobile batteries. The load demand will be completely met and at the minimum cost by targeting this objective function. The operator may also benefit from the price arbitrage, renewable curtailment mitigation, network expansion deferral, voltage drop mitigation, and loss reduction depending on the network situation as a result of the optimal spatial-temporal and power-energy scheduling of the TMMBs.

#### D. Second Stage: Emergency Operation

During severe events, the outage of network lines or power sources is quite probable. In this case, a portion of the load demand may leave unmet because of the supply shortage or network segmentation. The emergency operation state will be activated if the network is under such emergency situations, outage of distribution feeders, main substation, or distributed resources. The critical difference between this state with the previous one is generation inadequacy and/or network segmentation resulting in probable load shedding. In this case, there may be different ways to reduce the amount of the interrupted load depending on the available solutions. However, the maximum recovery rate of the disconnected load should be achieved at the minimum

expenses. For this purpose, a lexicographic planning model is developed. Accordingly, the maximum recoverable load is determined in the first step. In this case, the model first tries to maximize network resiliency by maximizing recovered load from the occurred event. To do this, the value of  $\psi$  is set to zero. As a result, the first term of the objective function introduced in (7) will be zero, and the remaining term denotes the total recovered load. The model now tries to retrieve as much as the load demand irrespective of the cost. After finding this value,  $E_{Tot}^{Shed}$ , the following constraint will be added to the model. It should be noted that this constraint is deactivated for the normal state since the unity value of  $\psi$ .

$$\sum_{i} \sum_{t} (1 - \zeta_{(i,t)}) P_{(i,t)}^{D} \ge (1 - \psi_{(t)}) E_{Tot}^{Shed}$$
 (8)

The above constraint denotes that the total recovered load demand has to be kept constant and the same as the previously found value. Having this new constraint, the objective function in (7) will then be again run by setting the value of  $\psi$  to one. Now, achieving the maximum resiliency operation schedule with the minimum operation expenses is ensured.

## E. Schedule Memory

The schedule memory is a new starting point for the horizon ahead and is related to the changes made to the TMMBs up to the current time period. The first parameter to be saved is the stored energy in the TMMBs at the end of the current time period. This parameter is easily saved and will act as the initial charge at the beginning of the next time period. The next parameter which has to be saved is the location of the TMMBs. In this case, there may be two situations. In the simplest case, where a TMMB has no displacement at the end of the current period, the current bus location will be regarded as the starting point for the next period. On the other hand, the TMMB may be on the road to connect to a new bus location during the present time period. In this case, the battery movement must be stored in such a way that it can be used at the beginning of the next period. For this purpose, a new virtual bus method is proposed. The concept of the virtual bus is shown in Fig. 4. In this method, the movement of each battery on the road is modeled by adding an isolated virtual bus.

Then, the TTTM transportation is adapted with this new bus. This bus is hypothetical and is not connected to the distribution network while located between the origin and destination buses of the previous transportation. In Fig. 4, it is assumed that a TMMB moves from bus A to bus B at the beginning of hour 1, and this transportation will take two hours. In this case, at the end of the first hour, when one hour of the required transportation time has elapsed, it can be assumed that the battery is located on a hypothetical bus, one hour away from the origin and destination buses. As a result, a new row and column must be added to the TTTM.

The entities of this new row and column are zero except for the two values, which means that this hypothetical bus is only connected to its beginning and end buses, A and B. Therefore, the two non-zero values corresponding to the distance of this hypothetical bus to the beginning and end of the movement,

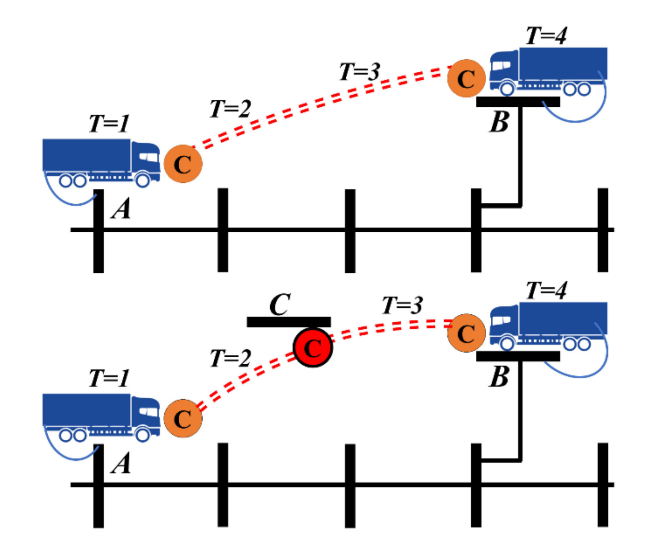


Fig. 4. A generic example of schedule memory.

i.e., buses A and B in our example, are equal to one hour. Thus, from the network operator viewpoint, the TMMB is in the hypothetical bus at the beginning of the next period. As a result, it can accept a new scheduling pattern by moving either to the origin or destination bus. In this way, the scheduling memory will be stored to be used at the beginning of the next time period.

Last but not least, it should be noted that the load shedding at *normal* operation state is not allowed dissimilar to the *Emergency* counterpart. These circumstances must be considered in the active and reactive power balance equations of the network buses. Accordingly, the power balance equations are arranged as follows.

$$\sum_{n} \Delta P_{(n,t)}^{S} + P_{(i,t)}^{R} + \sum_{b} P_{(b,i,t)}^{Di} = \sum_{b} P_{(b,i,t)}^{Ch} 
+ (1 - \zeta_{(i,t)}) P_{(i,t)}^{D} + \sum_{j} P_{(i,j,t)}^{F} \, \forall i \in A_{I}, \, \forall t \in A_{T} \quad (9)$$

$$\sum_{n} Q_{(n,t)}^{S} + Q_{(i,t)}^{R} + \sum_{b} Q_{(b,i,t)}^{Ca} = \sum_{b} Q_{(b,i,t)}^{In}$$

$$+ (1 - \zeta_{(i,t)}) Q_{(i,t)}^{D} + \sum_{j} Q_{(i,j,t)}^{F} \, \forall i \in A_{I}, \, \forall t \in A_{T}$$
(10)

The control over the on-off load switching during emergencies is built in the above equalities by deploying the  $\zeta$  variable. As a result, by setting the value of  $\zeta$  to zero in (9) and (10), there will be no chance for the model to manipulate load, denoting the *Normal* operation state. Otherwise, the model has complete control over loads at any time period employing the controllable value of  $\zeta$  in *the emergency* state.

Except for the developed model for the TMMBs, the following equations are required to model batteries and network behavior. In (11)–(13), the batteries are enforced to observe three limitations. The first one is that each battery can choose only one of the charging or discharging actions for the active power at any time period [23]. To mathematically model this constraint, two indicator auxiliary binary variables denote each of the

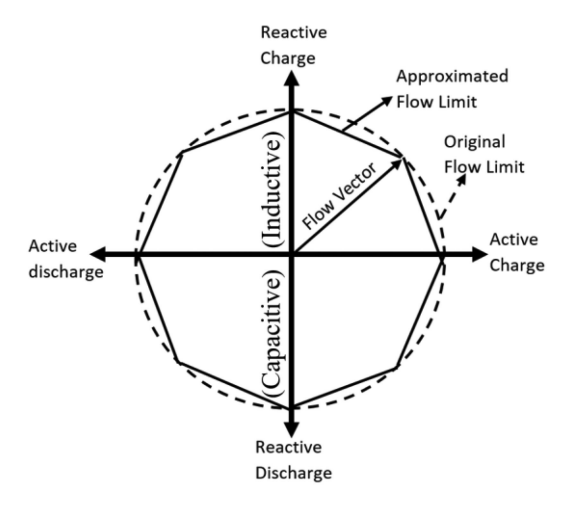


Fig. 5. Battery inverter flow limit and approximation by linear equations.

charging and discharging actions [24]. The second limitation over batteries operation is that they can exchange power with the grid if connected to one of the network buses. The third limitation is that the battery cannot exceed its power rating while charging or discharging. All of these limitations are modeled simultaneously in (11)–(13).

$$X_{(b,i,t)}^{PC} + X_{(b,i,t)}^{PD} \leq \Omega_{(b,i,t)}^{MB} \quad \forall b \in A_B, i \in A_I, \forall t \in A_T$$

$$(11)$$

$$0 \leq P_{(b,i,t)}^{Ch} \leq X_{(b,i,t)}^{PC} S_{(b)}^{MB} \quad \forall b \in A_B, i \in A_I, \forall t \in A_T$$

$$(12)$$

$$0 \le P_{(b,i,t)}^{Di} \le X_{(b,i,t)}^{PD} S_{(b)}^{MB} \quad \forall b \in A_B, i \in A_I, \forall t \in A_T$$
(13)

There is a similar situation for the reactive contribution of the batteries. As a result of employing the modern inverters for interfacing the storage cell with the AC grid, the battery system can contribute reactive power to the grid besides active power. Based on the manufacturers' data, available commercial battery systems can offer a full four-quadrant operation regime, as depicted in Fig. 5. As in the figure, the battery can inject or absorb reactive power while charging or discharging active power. In other words, the battery may work in one of the operation states: inductive reactive-active charging, inductive reactive-active discharging, capacitive reactive-active charging, and capacitive reactive-active discharging. The batteries can also work in either pure inductive or pure conductive state, similar to a parallel reactive or capacitor, benefiting from the full circle diagram. This capability is modeled while observing the above three limitations, similar to the active power. In (14)–(16), each battery is forced to choose only one of the inductive or capacitive reactive powers lower than its rated power if connected to one of the network buses.

$$Y_{(b,i,t)}^{QI} + Y_{(b,i,t)}^{QC} \le \Omega_{(b,i,t)}^{MB} \quad \forall b \in A_B, i \in A_I, \forall t \in A_T$$
(14)

$$0 \le Q_{(b,i,t)}^{In} \le Y_{(b,i,t)}^{QI} S_{(b)}^{MB} \quad \forall b \in A_B, i \in A_I, \forall t \in A_T$$
(15)

$$0 \le Q_{(b,i,t)}^{Ca} \le Y_{(b,i,t)}^{QC} S_{(b)}^{MB} \quad \forall b \in A_B, i \in A_I, \forall t \in A_T$$
(16)

The stored energy in the battery at any time period is a function of the previously stored value, and net energy exchange occurred at the present period. The net energy exchange is a function of the charging and discharging powers and corresponding efficiencies, as shown in (17). This stored energy has to observe minimum and maximum boundaries, modeled in (18).

$$J_{(b,t)}^{MB} = J_{(b,t-1)}^{MB} + \sum_{i} \left( P_{(b,i,t)}^{Ch} \eta_{(b)}^{Ch} \right) - \sum_{i} \left( P_{(b,i,t)}^{Di} / \eta_{(b)}^{Di} \right) \, \forall \, b \in A_B \,, \, t \in A_T \quad (17)$$

$$E_{(b)}^{Min} \le J_{(b,t)}^{MB} \le E_{(b)}^{Max} \quad \forall \ b \in A_B, \ t \in A_T$$
 (18)

The power rating limitation of the battery inverter has to be considered owing to the complex (active and reactive) nature of the power after the inverter. The conventional representation of this limitation is shown in (19). This equation denotes the position of the point inside a circle with the radius equal to the inverter power rating, as shown in Fig. 4 by a dashed line. Considering that the battery will contribute by one of the charging or discharging active powers at any time period, the net active power can be calculated by summing up these terms. Similarly, the net reactive power can be calculated by adding inductive and capacitive values. These substitutions are used to convert (19) to (20). The resulting equation is non-linear and has to be linearized to keep the linearity of the whole model. The method presented in [25] is used for this purpose. In this method, the main non-linear binding circle is approximated by a set of linear lines, as shown in Fig. 5. The approximation accuracy will enhance by increasing the number of straight lines (M) at the expense of the simulation run time. The linearized version of (20) using this method is shown in (21).

$$\sqrt{\left(P_{(b,i,t)}^{Net}\right)^{2} + \left(Q_{(b,i,t)}^{Net}\right)^{2}}$$

$$\leq S_{(b)}^{F} \quad \forall \quad b \in A_{B}, \quad \forall i \in A_{I}, \quad \forall t \in A_{T}$$

$$\sqrt{\left(P_{(b,i,t)}^{Ch} + P_{(b,i,t)}^{Di}\right)^{2} + \left(Q_{(b,i,t)}^{In} + Q_{(b,i,t)}^{Ca}\right)^{2}}$$

$$\leq S_{(b)}^{F} \quad \forall \quad b \in A_{B}, \quad \forall i \in A_{I}, \quad \forall t \in A_{T}$$

$$\leq S_{(b)}^{F} \quad \forall \quad b \in A_{B}, \quad \forall i \in A_{I}, \quad \forall t \in A_{T}$$

$$\leq S_{(b)}^{F} \quad \forall \quad b \in A_{B}, \quad \forall i \in A_{I}, \quad \forall t \in A_{T}$$

$$\leq S_{(b)}^{F} \quad \forall \quad b \in A_{B}, \quad \forall i \in A_{I}, \quad \forall t \in A_{T}$$

$$\leq S_{(b)}^{F} \quad \forall \quad b \in A_{B}, \quad \forall i \in A_{I}, \quad \forall t \in A_{T}$$

$$\leq S_{(b)}^{F} \quad \forall \quad b \in A_{B}, \quad \forall i \in A_{I}, \quad \forall t \in A_{T}$$

$$\leq S_{(b)}^{F} \quad \forall \quad b \in A_{B}, \quad \forall i \in A_{I}, \quad \forall t \in A_{T}$$

$$\leq S_{(b)}^{F} \quad \forall \quad b \in A_{B}, \quad \forall i \in A_{I}, \quad \forall t \in A_{T}$$

$$\leq S_{(b)}^{F} \quad \forall \quad b \in A_{B}, \quad \forall i \in A_{I}, \quad \forall t \in A_{T}$$

$$\leq S_{(b)}^{F} \quad \forall \quad b \in A_{B}, \quad \forall i \in A_{I}, \quad \forall t \in A_{T}$$

$$\leq S_{(b)}^{F} \quad \forall \quad b \in A_{B}, \quad \forall i \in A_{I}, \quad \forall t \in A_{T}$$

$$\leq S_{(b)}^{F} \quad \forall \quad b \in A_{B}, \quad \forall i \in A_{I}, \quad \forall t \in A_{T}$$

$$\leq S_{(b)}^{F} \quad \forall \quad b \in A_{B}, \quad \forall i \in A_{I}, \quad \forall t \in A_{T}$$

$$\leq S_{(b)}^{F} \quad \forall \quad b \in A_{B}, \quad \forall i \in A_{I}, \quad \forall t \in A_{T}$$

$$\leq S_{(b)}^{F} \quad \forall \quad b \in A_{B}, \quad \forall i \in A_{I}, \quad \forall t \in A_{T}$$

$$\leq S_{(b)}^{F} \quad \forall \quad b \in A_{B}, \quad \forall i \in A_{I}, \quad \forall t \in A_{T}$$

$$\leq S_{(b)}^{F} \quad \forall \quad b \in A_{B}, \quad \forall i \in A_{B}, \quad \forall i \in A_{T}$$

$$\frac{\cos\frac{(2m-1)\pi}{M}\left(P_{(b,i,t)}^{Ch} + P_{(b,i,t)}^{Di}\right) + \sin\frac{(2m-1)\pi}{M}\left(Q_{(b,i,t)}^{In} + Q_{(b,i,t)}^{Ca}\right)}{\cos\left(\pi/M\right)} \leq S_{(b)}^{MB} \\ \forall \ m \in A_M, \ b \in A_B, \ \forall \ i \in A_I, \ \forall \ t \in A_T$$
(21)

The same method is used in (22) for the network flow lines, wherein the apparent flow limit is limited to the line rating. The LinDistFlow equation in (21) is used to relate bus voltages with the line active and reactive power flow. The voltage magnitude limitations are enforced in (22) [26], [27]. Equality (23) denote

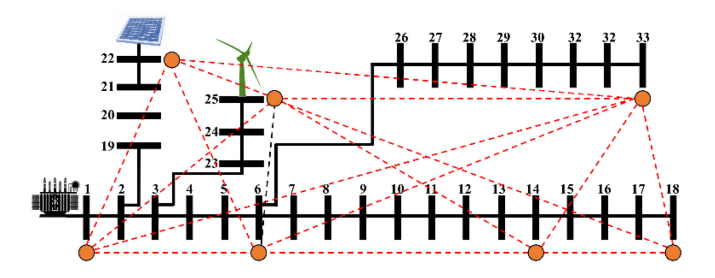


Fig. 6. The layout of the modified 33-bus distribution test system coupled with a transportation network.

the relation between maximum, generated, and curtailed renewable energy, and finally (24) limits the reactive power generation of renewable resources to the maximum allowable value [28].

$$\frac{\cos\frac{(2m-1)\pi}{M}\left(P_{(i,j,t)}^{F}\right) + \sin\frac{(2m-1)\pi}{M}\left(Q_{(i,j,t)}^{F}\right)}{\cos(\pi/M)} \leq S_{(i,j)}^{F}$$

$$\forall m \in A_{M}, \forall i, j \in A_{I}, \forall t \in A_{T}$$

$$2\left(R_{(i,j)}^{F}P_{(i,j,t)}^{F} + X_{(i,j)}^{F}Q_{(i,j,t)}^{F}\right)$$
(22)

$$V_{Min}^{Bus} \le V_{(i,t)} \le V_{Max}^{Bus} \ \forall i \in A_I, \forall t \in A_T$$
 (24)

 $= V_{(i,t)} - V_{(i,t)} \ \forall \ \{i,j\} \in A_I, \ \forall \ t \in A_T$ 

$$P_{(i,t)}^{R} = P_{R(i,t)}^{Max} + P_{R(i,t)}^{Cut} \qquad \forall i \in A_I, \forall t \in A_T$$
 (25)

$$Q_{(i,t)}^{R} \leq \tan\left(Arc\left(\cos PF_{(i)}^{R}\right)\right) \qquad \forall i \in A_{I}, \, \forall \, t \in A_{T}$$
(26)

## III. CASE STUDY

A modified version of the 33-bus distribution test system is used to implement the proposed model. Fig. 6 shows the original system configuration along with the modifications. As in the figure, two distributed generation resources in the form of the solar PV and wind turbines are added to, in turn, buses 22 and 25. It is assumed that the distributed generation resources belong to the system operator, and as a result, their power generation cost is zero. The system is also enhanced with two TMMB, TMMB#1 and TMMB#2, each with a 500 kW power rating and capable of storing 10–90% of its 1000 kWh nominal energy capacity.

The TMMBs start the daily operation schedule with 10% initial stored energy from Bus#1 and 90% charging and discharging efficiencies. Besides, a road transportation network is mapped into the existing distribution network with the intersection (connection) points at buses 1, 6, 14, 18, 22, 25, and 33. The minimum distance of the routes, shown by the dashed line in the figure, is calculated based on the idea introduced in Section II. For simplicity and a clear comparison with the emergency case, it is assumed that traveling from one connection bus to another takes one hour. In other words, all of the entries except for the main diameter (which is equal to zero) in TTTM are equal to one. Each hour of transportation of the TMMBs costs 10 \$. This means the same value for each bus connection change considering a one-hour transportation duration for all candidates. The line and load data of the system, along with the stair-wise substation cost function, are provided in [29]. The

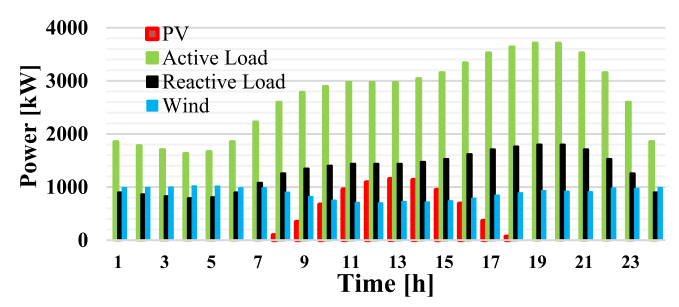


Fig. 7. Hourly profile of the load demand and renewable resources generation.

TABLE I
MAIN SIMULATION RESULTS FOR NORMAL PRE-DISASTER SCENARIO

Case		With MB	No MB	
	Generation	5,984	6,458	
Cost (\$)	Batteries	50	-	
	Total	6,034	6,458	
Renewable	PV	0	1,317	
Curtailment	Wind	96.6	393	
(kWh)	Total	96.6	1,710	
Transports	TMMB#1	3 (2, 13, 16)	-	
# (Bus)	TMMB#2	2 (4, 16)	-	

capacity of the lines connecting distributed resources laterals, i.e., lines connecting buses 2-19 and 3-12, is reduced to 500 kVA to simulate renewable energy curtailment because of line overload. Fig. 7 demonstrates hourly forecasted values for the active and reactive load demand and renewable resources generation. The proposed model is implemented on the described system in three subsequent scenarios, namely normal pre-disaster, resilient emergency, and normal post-disaster, described in the following. The model is implemented in GAMS and solved using the CPLEX [30].

## A. Pre-Disaster Normal Operation

The previously described system starts the daily operation horizon with the profiles shown in Fig. 7. The main simulation results, operation cost, and renewable curtailment for this scenario with and without mobile batteries are given in Table I.

Employing the TMMBs affects the network operation in two ways, operation cost and renewable curtailment. Based on the results, the TMMBs utilization has resolved PV curtailment completely, i.e., 1317 kWh. On the other hand, wind energy curtailment has experienced a 296 kWh reduction. As a result, a value of 1613 kWh of curtailed renewable energy is recovered via TMMBs. This energy recovery and the price arbitrage performed by the mobile batteries have resulted in a daily operation cost reduction of 501 \$, equal to more than 7.7%. This achievement is realized at the expense of a 50 \$ payment for TMMBs transportation.

Fig. 8 presents the share of each resource in the hourly curtailed renewable energy for both cases. As can be observed from the figure, the Wind-MB orange bars, positive values, stand for wind energy curtailment energy when employing mobile batteries. It should be noted that the solar energy curtailment will be completely recovered via employing mobile batteries. On the

(23)

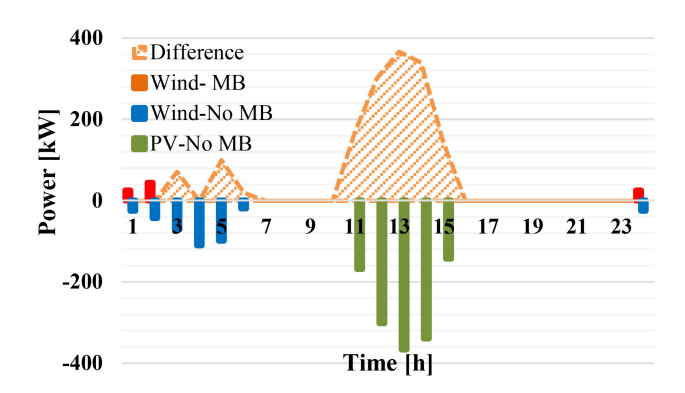


Fig. 8. Hourly curtailed renewable energy by source for normal state.

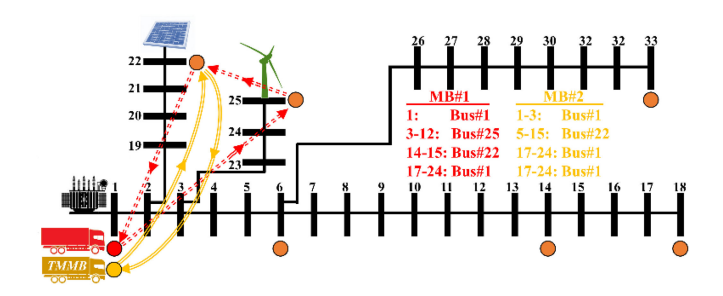


Fig. 9. Transportation schedule of the TMMBs for normal state.

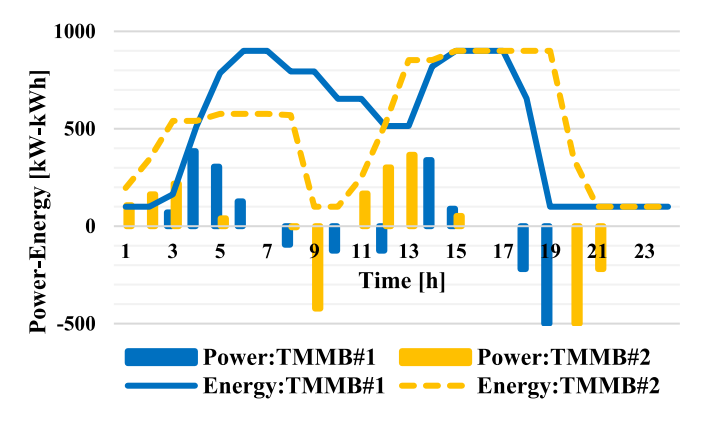


Fig. 10. Hourly power and energy schedule of the batteries for the normal state.

contrary, the negative values, blue and green bars in the figure denote, in turn, wind and solar energy curtailment for the system without mobile batteries. The positive hatched area demonstrates the total hourly renewable curtailment difference between both cases. As can be observed, utilization of the TMMBs has resulted in retrieving curtailed renewable energy entirely except for the wind energy curtailment at hours 1, 2, and 24. The failure of the mobile batteries to cope with the curtailment at these hours is related to the required initial and final inevitable transportation times. In other words, the batteries will fail to capture curtailed energy during these hours because of being on the roads from the and coming back to the initial location. The three last rows of Table I present the transportation schedule of the TMMBs along with the connection buses. In addition, Figs. 9 and 10 demonstrate the connection-transportation and power-energy schedule of the TMMBs, respectively. Based on the results and as expected, both of the TMMBs have selected the buses

with renewable curtailment mitigation opportunities to connect, namely buses 22 and 25. TMMB#2 has experienced a different schedule since it has been charged during the first three hours at its initial location, Bus#1. Then, it has moved at hour 4 to be at Bus#22. It has connected to this bus near PV during hours 5-15.

In this bus, the battery is first charged at hour 5, and then it discharges the stored energy during hours 8 and 9. After that, it reached its energy storage capacity by charging during hours 10-13 and 15. The stored energy from solar power is retrieved from curtailment by moving TMMB#2 to Bus#1 during hour 16 to meet a considerable share of the power demand. Accordingly, MB#1 has only been in its initial location, Bus#1, for the first hour. Then, it has been on the road during the second hour to be at the beginning of the third hour at the wind farm location, i.e., Bus#25. After being connected in this place, it is charged during hours 3-6. A part of the stored energy is then released at hours 8, 10, and 12. In this way, the battery has prevented the nontransferable wind energy from being cut off by performing a time shift. Then, the battery was transported during hour 13 to be at the solar power bus location right from its peak production, i.e., hour 14. After being connected near the solar power plant, the battery has absorbed most of the exposure to curtail solar energy at hours 14 and 15. After that, the battery has moved at hour 16 to its original location, Bus# 1, to deliver the stored energy during peak load hours. The stored solar energy is ultimately delivered during the peak load period, hours 18 and 19. As a result, TMMB#1 has mitigated the renewable energy curtailment by performing a temporal shift on wind energy and a spatial and temporal shift on solar energy. Accordingly, TMMB#2 has performed a price arbitrage benefiting from substation energy at a lower cost at the initial hours of the operation. Then, a considerable share of the solar energy is retrieved by performing a temporal-spatial shift. The battery in this cycle has recovered most of the non-transferable and exposed to curtailment solar energy by transferring from bus 22 to Bus#1 during peak hours.

#### B. Resilient Emergency Operation

The proposed operation paradigm found in the previous section, based on the flowchart shown in Fig. 1, will be implemented on the system hour by hour in practice, and at the end of each hour, the schedule memory is stored. During each hour, the new information received will be analyzed and included in the operation of the future system periods, as discussed earlier. It is assumed that the system will be operated without any changes and based on the obtained schedule by the end of the third hour. However, there will be an accident for the system during hour four, causing diverse consequences.

The repair crew examination determines that the complete system recovery will last until the end of hour 15. This means that there is an emergency state operation period between hours 5-15. It should be noted that this assumption is for the simple analysis of the results, and any other dynamics such as step-by-step repair of lines and roads can be considered owing to the proposed model flexibility. The event, which can be based on various internal or external factors, has diverse consequences on electricity and transportation networks, as shown in Table II. According to the table, the incident will cause the outage of three lines (19-2,

TABLE II
CONSEQUENCES OF THE OCCURRED EVENT

Network	Event	Consequence	
		Line 2-19	
Distribution	Line outage	Line 3-23	
		Line 6-26	
	Connection	Outage of	
Transportation	location outage	Bus #6	
	Road	Doubling each	
	congestion	Travel time and cost	

TABLE III
MODIFIED VERSION OF THE TOTAL TRANSPORTATION TIME

	1	6	14	18	22	25	33	34
1	0	<u>24</u>	2	2	2	2	2	1
6	<u>24</u>	0	<u>24</u>	<u>24</u>	<u>24</u>	<u>24</u>	<u>24</u>	<u>24</u>
14	2	<u>24</u>	0	2	2	2	2	24
18	2	<u>24</u>	2	0	2	2	2	24
22	2	<u>24</u>	2	2	0	2	2	2
25	2	<u>24</u>	2	2	2	0	2	24
33	2	<u>24</u>	2	2	2	2	0	24
34	1	<u>24</u>	24	24	1	24	24	0

23-3, and 26-6), the loss of the connection point in Bus#6, and also doubling the transportation time and cost between other connection points. As it was introduced, the schedule memory for the current hour must first be defined and stored. Accordingly, TMMB#1 at the beginning of the emergency operation, i.e., hour 5, will be in bus 22 and with 510.5 kWh stored energy. As a result, these conditions will be considered as the initial status of this battery at the beginning of the emergency operation period. There are different conditions for TMMB#2, considering that it moved in the last hour before the event. Due to increased road congestion and enhanced transportation time, TMMB#2 will not reach its destination after one hour. Therefore, it is necessary to model the initial conditions for this battery based on the proposed virtual bus method. As a result, an additional hypothetical bus will be added to the TTTM without any connection to other network buses, i.e., bus number 34. It is supposed that TMMB#2 is located in this hypothetical bus at the beginning of hour 5 with a stored energy of 541 kWh. This situation mimics the previous transportation state of the battery. The virtual new bus is connected through road lines only to the beginning and ending locations of the battery movement before the event, i.e., Bus#1 and Bus#2, respectively. Since expiring one hour out of the two hours required transportation time, the distance of this hypothetical bus from the two mentioned buses will be considered equal to one hour to be in line with the new two-hour transportation time. Also, the lack of connection of the new bus with other connection points in the network and also the lack of availability of bus 6 for connection has been modeled by increasing the transportation time to 24 hours. Table III presents the modified TTTM for the emergency state operation considering a new virtual bus. The proposed model is simulated from hour 5 to hour 15 with the abovementioned initial conditions and based on the emergency state operation paradigm.

TABLE IV
MAIN SIMULATION RESULTS FOR EMERGENCY OPERATION SCENARIO

Case		With MB	No MB	
Total Shed Load (kWh)		6,067	8,335	
	Generation	1,571	1,571	
Cost (\$)	Batteries	90	-	
	Total	1,641	1,571	
Renewable	PV	2,901	4,315	
Curtailment	Wind	1,698	2,131	
(kWh)	Total	4599	6,446	
Transports	TMMB#1	3 (25, 22, 33)	-	
# (Buses)	TMMB#2	2 (34*,22, 33)	-	

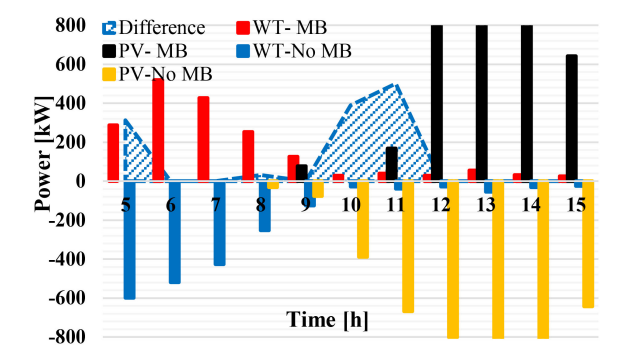


Fig. 11. Hourly curtailed renewable energy for emergency state with and without TMMBs.

The main simulation results for this case with and without the mobile batteries are shown in Table IV. The table contains the total shed load, wind, PV, and the total curtailed renewable energy, along with the transportation and bus connection of the mobile batteries. As in the table, the total unmet load has experienced a reduction from 8335 kWh to 6067 kWh, denoting a 2553 kWh decline equal to more than 30%. This reduction in the shed load is achieved by optimal TMMBS scheduling at the expense of a 90 \$ transportation cost. Considering the isolated situation of Zone 1, the injected power from the substation and the resulting cost remained the same in both cases, i.e., 1571 \\$. The reduction in the unmet load performed by the mobile batteries is achieved by storing and transporting excess renewable energy. In other words, the TMMBs have recovered the excess renewable energy to meet a portion of the load demand at Zone 4 without any power sources. As a result, the wind and PV curtailment has, in turn, reduced by 433 kWh and 1414 kWh resulting in a 28.65% reduction in the total curtailed energy. To achieve these results, TMMB#1 has experienced three transportations between buses 22, 25, and 33, while TMMB#2 has had two transportations between buses 34 (virtual), 22, and 33.

Fig. 11 depicts the share of each renewable resource in the hourly curtailed renewable energy for both cases. In the figure, the positive and negative values denote the cases wherein the mobile batteries are deployed and not, respectively. As can be seen, the TMMBs deployment has reduced curtailed renewable energy in three periods, namely hours 5, 8, and 9-12. The TMMBs have recovered the wind energy during the initial hours of the emergency state and the solar energy during midday hours.

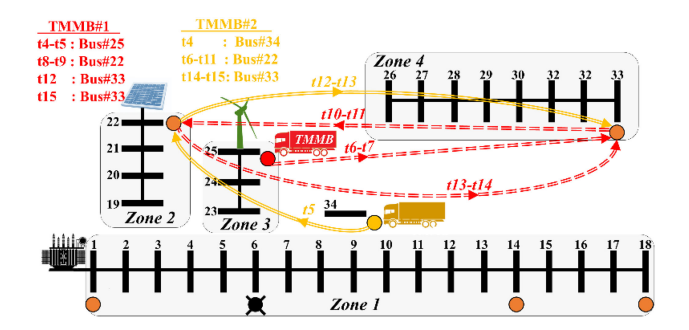


Fig. 12. Power and energy schedule of the batteries for the emergency state.

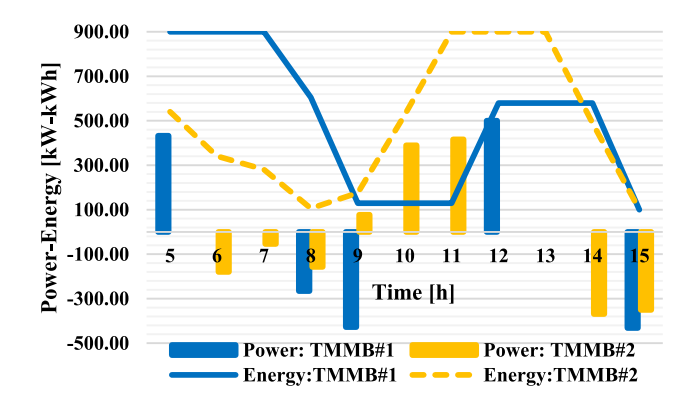


Fig. 13. Hourly total system power balance for the emergency state.

The batteries have failed to capture excess renewable energy at other hours since they have been discharged for some hours.

Fig. 12 demonstrates the spatiotemporal status of the TMMBs during the emergency operation state. Also, Fig. 13 shows the charging and discharging powers and the stored energy in each TMMB for the same scenario. Based on the results, both batteries behave similarly, transferring energy from surplus to deficient zones. In other words, both batteries have stored and transported excess energy from Zone 2 (PV panels) and Zone 3 (wind turbines) to Zone 3 (without source).

As shown in the figure, only Zone 1 has a dispatchable and adequate power supply, the main substation. Other zones in the network have been isolated from the substation. Although Zone 2 and Zone 3 are installed with, in turn, solar and wind resources, Zone 4 does not possess any power source. Besides, it should be noted that only the wind turbines can entirely meet the load demand of Zone 3. In other words, the power supply is deficient in Zone 2 during the initial hours of the day without solar radiation. Accordingly, the TMMBs have attempted to compensate for the supply shortage in Zone 2 and Zone 4. TMMB#1 spends the first hour of emergency state in its initial location and charging from excess wind energy, namely Bus#25. Then, it has used stored energy to supply a portion of the load demand in Zone 4 by being on the road during hours 6 and 7. Accordingly, TMMB#1 has discharged stored energy from hours 8 to 9 in Bus#33 of Zone 3. After depleting the stored energy, it has moved to Bus#22 in Zone 2 to benefit from the excess solar energy. To do this, TMMB#1 has been transported during hours 10 and 11 to be in the PV panel location. It has

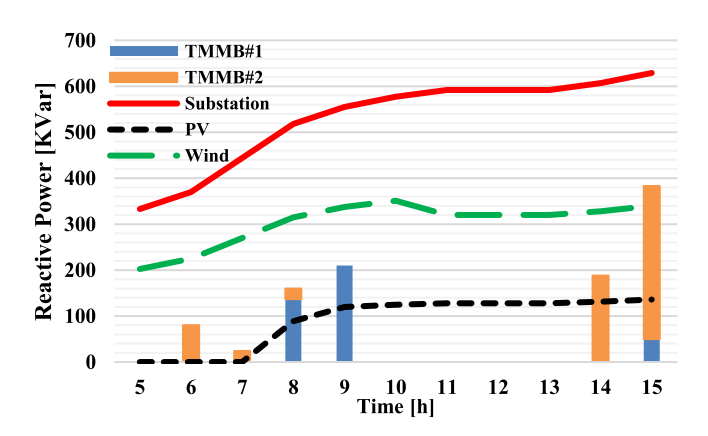


Fig. 14. Reactive power exchange of the TMMBs during emergency operation.

been charged in this location for one hour and then moved back to Bus#3. The battery has been on the road during hours 13 and 14 to discharge stored energy at hour 15 in Bus#33 in Zone 4. As a result, TMMB#1 has experienced three transportations to meet a portion of the unmet load in Zone 4.

On the other hand, TMMB#2 has continued moving from the previous hour to reach its destination at Bus#22 in Zone 2. It is then discharged in this zone during hours 6 to 8 to meet a part of the power demand when sun radiation is deficient. The TMMB#2 is then charged during hours 9-11 when it has access to the PV panels' excess energy. Subsequently, it has been transported from hour 12 to hour 13 to be at Bus#33 at the beginning of hour 14. After connecting to its destination in Zone 4, TMMB#2 is discharged during hours 14-15 to provide a share of the load demand. This way, TMMB#2 has reduced some of the shed load in Zones 2 and 4 by shifting required energy spatially and temporally.

Fig. 14 shows the reactive power provided by the available sources in the network, i.e., upstream substation, distributed renewable resources, and mobile batteries. As explained previously, the TMMBs can work either in inductive or capacitive reactive mode. Based on the results, The network state was such that there was no need to absorb reactive power by the mobile batteries. In other words, the network never faces an overvoltage during emergency operation, which requires reactive power absorption to handle. As a result, all reactive power sources in the network, including mobile batteries, have always been injected the reactive power or, equivalently, have worked in the capacitive reactive mode. Another point is that the TMMBs have injected reactive power during hours with lower active power flow. In other words, the batteries at hours with free apparent power capacity have used this opportunity to inject reactive power and meet a portion of the reactive demand.

#### C. Post-Disaster Normal Operation

After repairing the damages, the network will return to its normal operation state. The post-disaster normal operation state commences at the beginning of hour 16. In this situation, the distribution grid topology and transportation network routes are the same as the original condition shown in Fig. 6. The only difference is that both TMMBs are now in Bus#33. There are

two points related to the second stage of the network operation, namely the post-disaster situation. The first one is that the batteries must be relocated to the initial location and the initial stored energy. The second point is that the entries of the TTTM are now the same and equal to one hour. Simulating the system for this stage demonstrates a total 3829 \$ operation cost, without load shedding, and 25 kWh of curtailed wind energy. Both TMMBs have transported from Bus#33 to Bus#1 during hours 22 and 20, respectively. In this stage, only TMMB#1 has charged 135 kW once at hour 16 and then discharged the stored energy at hour 20. The critical point about this schedule to be pointed out is that it is entirely in accordance with load and renewable profiles. In other words, there is no considerable opportunity for renewable curtailment mitigation at this stage on the one hand. On the other hand, the shape of the load profile in this stage, i.e., hours 16-24, is such that there is no chance for price arbitrage regarding declining load demand. These facts are the reason for the relative inactivity of the batteries during this period. The results also indicate that the spatial-temporal and power-energy schedule of the batteries is entirely consistent with the joint distribution-transportation network status and operator preferences.

## IV. CONCLUSION

Accordingly, these devices' optimal modeling and scheduling in a coupled distribution-transportation network were targeted by proposing a combined normal-emergency operation paradigm. The proposed model handled scheduling uncertainties through a new schedule memory concept integrated into a rolling horizon approach. The model's performance was tested in a three-stage scenario chain, including normal pre-disaster, resilient emergency, and normal post-disaster operation. The case study results demonstrated a 6.5% reduction in the total operation cost comprising a renewable energy recovery rate of 94.5%. Following the consequences of an event, the spatialtemporal and energy-energy schedule of the batteries altered to adapt to the new network changes. As a result, the batteries transferred exposed to curtail renewable energy, spatially and temporally, to the area without an energy source to increase system flexibility and at an affordable cost. The resilient operation schedule resulted in a 30% reduction in unmet load besides more than 20% in the renewable energy curtailment retrieval. As future trends, this study can be continued by evaluating the effect of repositioning the mobile resources on system flexibility before extreme events using machine learning techniques. Additionally, a hybrid short-long term mobile storage system modeling and scheduling composed of hydrogen tanks and mobile batteries can be addressed.

## REFERENCES

- J. Ramsebner, R. Haas, A. Ajanovic, and M. Wietschel, "The sector coupling concept: A critical review," Wiley Interdiscipl. Rev.: Energy Environ., vol. 10, no. 4, 2021, Art. no. e396.
- [2] P. Palensky and D. Dietrich, "Demand side management: Demand ressponse, intelligent energy systems, and smart loads," *IEEE Trans. Ind. Inform.*, vol. 7, no. 3, pp. 381–388, Aug. 2011.

- [3] M. T. Van Vliet, D. Wiberg, S. Leduc, and K. Riahi, "Power-generation system vulnerability and adaptation to changes in climate and water resources," *Nat. Climate Change*, vol. 6, no. 4, pp. 375–380, 2016.
- [4] V. B. Venkateswaran, D. K. Saini, and M. Sharma, "Approaches for optimal planning of energy storage units in distribution network and their impacts on system resiliency," *CSEE J. Power Energy Syst.*, vol. 6, no. 4, pp. 816–833, 2020.
- [5] H. Saboori, R. Hemmati, S. M. S. Ghiasi, and S. Dehghan, "Energy storage planning in electric power distribution networks—a state-of-the-art review," *Renewable Sustain. Energy Rev.*, vol. 79, pp. 1108–1121, 2017.
- [6] M. Hiremath, K. Derendorf, and T. Vogt, "Comparative life cycle assessment of battery storage systems for stationary applications," *Environ. Sci. Technol.*, vol. 49, no. 8, pp. 4825–4833, 2015.
- [7] H. Saboori and S. Jadid, "Optimal scheduling of mobile utility-scale battery energy storage systems in electric power distribution networks," *J. Energy Storage*, vol. 31, 2020, Art. no. 101615.
- [8] G. He, J. Michalek, S. Kar, Q. Chen, D. Zhang, and J. F. Whitacre, "Utility-scale portable energy storage systems," *Joule*, vol. 5, no. 2, pp. 379–392, 2021.
- [9] H. Saboori, S. Jadid, and M. Savaghebi, "Spatio-Temporal and powerenergy scheduling of mobile battery storage for mitigating wind and solar energy curtailment in distribution networks," *Energies*, vol. 14, no. 16, 2021, Art. no. 483.
- [10] H. Saboori and S. Jadid, "Capturing curtailed renewable energy in electric power distribution networks via mobile battery storage fleet," *J. Energy Storage*, vol. 46, 2022, Art. no. 103883.
- [11] J. Kim and Y. Dvorkin, "Enhancing distribution system resilience with mobile energy storage and microgrids," *IEEE Trans. Smart Grid*, vol. 10, no. 5, pp. 4996–5006, Sep. 2018.
- [12] S. Lei, C. Chen, Y. Li, and Y. Hou, "Resilient disaster recovery logistics of distribution systems: Co-optimize service restoration with repair crew and mobile power source dispatch," *IEEE Trans. Smart Grid*, vol. 10, no. 6, pp. 6187–6202, Nov. 2019.
- [13] L. Jiang et al., "Resilient service restoration for distribution systems with mobile resources using Floyd-based network simplification method," *IET Gener. Transmiss. Distrib.*, vol. 16, pp. 414–429, 2021.
- [14] S. Yao, P. Wang, X. Liu, H. Zhang, and T. Zhao, "Rolling optimization of mobile energy storage fleets for resilient service restoration," *IEEE Trans. Smart Grid*, vol. 11, no. 2, pp. 1030–1043, Mar. 2019.
- [15] S. Lei, C. Chen, H. Zhou, and Y. Hou, "Routing and scheduling of mobile power sources for distribution system resilience enhancement," *IEEE Trans. Smart Grid*, vol. 10, no. 5, pp. 5650–5662, Sep. 2019.
- [16] P. Prabawa and D.-H. Choi, "Multi-agent framework for service restoration in distribution systems with distributed generators and static/mobile energy storage systems," *IEEE Access*, vol. 8, pp. 51 736–51 752, 2020.
- [17] S. Yao, P. Wang, and T. Zhao, "Transportable energy storage for more resilient distribution systems with multiple microgrids," *IEEE Trans. Smart Grid*, vol. 10, no. 3, pp. 3331–3341, May 2019.
- [18] M. Nazemi, P. Dehghanian, X. Lu, and C. Chen, "Uncertainty-aware deployment of mobile energy storage systems for distribution grid resilience," *IEEE Trans. Smart Grid*, vol. 12, no. 4, pp. 3200–3214, Jul. 2021.
- [19] Z. Qu, J. Chen, K. Peng, Y. Zhao, Z. Rong, and M. Zhang, "Enhancing stochastic multi-microgrid operational flexibility with mobile energy storage system and power transaction," *Sustain. Cities Soc.*, vol. 71, 2021, Art. no. 102962.
- [20] X. Liu, C. B. Soh, T. Zhao, and P. Wang, "Stochastic scheduling of mobile energy storage in coupled distribution and transportation networks for conversion capacity enhancement," *IEEE Trans. Smart Grid*, vol. 12, no. 1, pp. 117–130, Jan. 2021.
- [21] H. Saboori and S. Jadid, "Mobile and self-powered battery energy storage system in distribution networks—modeling, operation optimization, and comparison with stationary counterpart," *J. Energy Storage*, vol. 42, 2021, Art. no. 103068.
- [22] Y. Zheng, K. Meng, F. Luo, J. Qiu, and J. Zhao, "Optimal integration of MBESSS/SBESSS in distribution systems with renewables," *IET Renewable Power Gener.*, vol. 12, no. 10, pp. 1172–1179, 2018.
- [23] Y. Sun, Z. Li, M. Shahidehpour, and B. Ai, "Battery-based energy storage transportation for enhancing power system economics and security," *IEEE Trans. Smart Grid*, vol. 6, no. 5, pp. 2395–2402, Sep. 2015.
- [24] S. Dehghan and N. Amjady, "Robust transmission and energy storage expansion planning in wind farm-integrated power systems considering transmission switching," *IEEE Trans. Sustain. Energy*, vol. 7, no. 2, pp. 765–774, Apr. 2016.

- [25] M. Nick, R. Cherkaoui, and M. Paolone, "Optimal allocation of dispersed energy storage systems in active distribution networks for energy balance and grid support," *IEEE Trans. Power Syst.*, vol. 29, no. 5, pp. 2300–2310, Sep. 2014.
- [26] M. E. Baran and F. F. Wu, "Network reconfiguration in distribution systems for loss reduction and load balancing," *IEEE Power Eng. Rev.*, vol. 9, no. 4, pp. 101–102, Apr. 1989.
- [27] A. M. Nakiganda, S. Dehghan, and P. Aristidou, "Comparison of ac optimal power flow methods in low-voltage distribution networks," in *Proc. IEEE PES Innov. Smart Grid Technol. Europe*, 2021, pp. 1–5.
- [28] Y. Sun, J. Zhong, Z. Li, W. Tian, and M. Shahidehpour, "Stochastic scheduling of battery-based energy storage transportation system with the penetration of wind power," *IEEE Trans. Sustain. Energy*, vol. 8, no. 1, pp. 135–144, Jan. 2017.
- [29] H. Mehrjerdi and R. Hemmati, "Modeling and optimal scheduling of battery energy storage systems in electric power distribution networks," *J. Cleaner Prod.*, vol. 234, pp. 810–821, 2019.
- [30] R. E. Rosenthal, Gams-A User's Guide. WA, DC, USA: GAMS Development Corporation, 2004.



Hasan Mehrjerdi (Senior Member, IEEE) received the B.Sc. degree from the Ferdowsi University of Mashhad, Mashhad, Iran, in 1998, the M.Sc. degree from Tarbiat Modares University, Tehran, Iran, in 2002, and the Ph.D. degree from Quebec University (École de technologie supérieure), Montreal, QC, Canada, in 2010, all in electrical engineering. From 2011 to 2013, he was with the Power Systems and Mathematics Department, Research Institute of Hydro-Quebec, Varennes, QC, Canada. He was a Senior Power System Researcher with Abengoa Re-

search, Sevilla, Spain, in 2014. He is currently a Distinguished Associate Professor with the Electrical Engineering Department, Qatar University, Doha, Qatar. His research interests include intelligent power systems, renewable energy, energy storage, and protection studies. He was among the world's top 2% scientist based on standardized citation indication in Energy in 2020 and 2021. The list was completed by Stanford University, CA, USA.



Hedayat Saboori received the Ph.D. degree from the Iran University of Science and Technology, Tehran, Iran, in 2022. He is currently an Assistant Professor with the Electrical Engineering Department, Kermanshah University of Technology, Kermanshah, Iran. His research interests include technology and application of grid-scale mobile and stationary energy storage systems, operation and planning of distributed and renewable energy resources, and sustainable and smart energy systems analysis and design.



Shahram Jadid received the Ph.D. degree from the Indian Institute of Technology, Mumbai, India, in 1991. He is currently a Professor with the Department of Electrical Engineering, Iran University of Science and Technology, Tehran, where he is also a member of the Center of Excellence for Power System Automation and Operation (CEPSAO). His research interests include smart grids, power system operation and restructuring, and load and energy management. He is the Editor-in-Chief of the *Iranian Journal of Electrical and Electronic Engineering* (IJEEE).